Progress In Electromagnetics Research M, Vol. 112, 41–53, 2022

Multi-Beam Forming and Optimization for Active Phased Array Antenna Using Genetic Algorithm

Ji-Hoon Bae[1, *] and Won Kyu Choi[2]

Abstract—In this paper, the optimized results of multi-beam forming for an active phased array antenna are presented. In the case of a horn radiator, to implement equal main beamwidths and a low side-lobe level in the principal planes, a circularly polarized dual-mode horn antenna with the gain over 14.5 dBi is designed and fabricated at the Ka-band, which is composed of a conical horn, polarizer, and transducer. In the case of multi-beam forming, when several main beams are simultaneously generated within a limited scanning range, large side-lobes can be observed among the main beams. To overcome this phenomenon, an evolutionary technique, such as a genetic algorithm, is applied to the optimization of a multi-beam pattern. It is shown that the proposed method can significantly reduce the outer side-lobe level as well as the inner side-lobe level of the simultaneous multi-beam pattern.

1. INTRODUCTION

Active phased array antennas (APAA) for the geostationary orbit (GEO) or the low earth orbit (LEO) have been studied and developed for several decades. With increased demand for ultra-wideband and multimedia services, such as Internet, VOD (video on demand), satellite broadcasting, and remote-education, steerable multi-beam antennas have become a core technology in satellite communication systems [1–5]. Therefore, it is preferable to use a multi-beam APAA (MAPAA) system rather than a single-beam antenna system to provide various services of high quality and to adaptively meet some changes of the service environment between ground networks and satellite networks. Also, recently, multi-beamforming systems have been actively used in mm-wave band. A beam scheduling algorithm using measurements of receiving power was introduced to improve latency in [6], and the model-free multi-beam tracking algorithm combining the Q-learning with auxiliary beam pair-based angle estimation in mm-wave band was devised in [7].

In this paper, we focus on the optimal design of a circularly polarized horn antenna and the implementation and optimization of multi-beam patterns for the transmitting MAPAA. First, the circularly polarized dual-mode horn antenna designed in this paper is composed of a conical horn, polarizer, and transducer. The dual-mode in the conical horn is excited by a waveguide feed with internal bifurcation junction. The polarizer with a metallic wedge is designed to produce a circular polarization with low axial ratio characteristics. Generally, traditional rectangular horn antennas operating in the dominant TE_{10} mode and conical horn antennas in the TE_{11} mode have different beamwidths in the principal planes. This is due to the remarkably different field distributions that are uniform in the E-plane but nonuniform in the H-plane [8]. In addition, because of the aperture phase errors caused by the spherical phase fronts, equal principal plane patterns cannot be achieved over a wide frequency band. A wider bandwidth with equal beamwidths and low cross-polarization in the principal planes can be accomplished by employing higher order modes [8, 9]. By exciting the horn aperture with a proper

Received 29 May 2022, Accepted 8 July 2022, Scheduled 24 July 2022

* Corresponding author: Ji-Hoon Bae (jihbae@cu.ac.kr).

[1] Department of AI and Big Data Engineering, Daegu Catholic University, Republic of Korea. [2] Electronics and Telecommunications Research Institute, Korea.

combination of TE_{11} and TM_{11} modes, it is possible to produce radiation patterns with approximately equal beamwidths in the E- and H-planes, as well as the side-lobe levels (SLLs) in the E-plane lower than those of horns excited by a single mode. In this study, to obtain the same beamwidths in two principal planes, the length of an inner waveguide is optimally adjusted using the commercial software tool, High-Frequency Structure Simulator (HFSS) [10].

In the case of multi-beam synthesis, when several main beams are generated for each differently predetermined beam direction at the same time, large inner side-lobes can appear among the main beams. To overcome this problem, a genetic algorithm (GA) [11] is applied to the optimization of the multi-beam pattern for simultaneous reduction of outer side-lobes as well as inner side-lobes. GA is a global optimization method modeled on the Darwinian natural selection and evolution concepts. Application-specific GA schemes have attracted electromagnetics researchers by effectively solving complex and challenging optimization problems on electromagnetic systems. Therefore, GA is widely applied and used in various fields even to this day. For example, in the field of satellite communication systems, the authors in [4] solved the joint power and bandwidth allocation optimization problem by using GA, and the dynamic beam hopping method to improve resource utilization is studied based on GA [5]. In addition, a desired low SLL can be accomplished by optimally adjusting either the excitation of each antenna element or the elements' positions with uniform amplitudes [12–17]. The excitation includes the amplitudes and phases of antenna elements. Because it is difficult to construct sub-array modules and to implement a simple array antenna system in the latter method, we adopt the former method for the transmitting MAPAA. To control the amplitudes and phases of antenna elements, the amplitudes and phases of four channels in an active beamforming module (ABFM) must be adjusted to the desired values for each specific direction. Our designed ABFM has four input channels, which have their own phase shifter and variable attenuator [18]. In the developed transmitting antenna system, when the amplitudes of each channel in the ABFM are adjusted using each attenuator, the phases in each channel can also be varied, leading to phase variation of the channel. Due to the effect of this phase variation, the main beam direction can deviate from the desired one, or radiation patterns adversely distorted. Because of this phenomenon, only the phases of each antenna element are optimized using each phase shifter, while all the amplitudes have fixed values during the optimization procedure. The main contributions of this study are as follows:

1) A formula for designing a multi-beam-forming structure with a triangular lattice was derived and presented, and based on this, it was reflected in the actual MAPAA system design and fabrication using four-channel ABFMs.
2) The circularly polarized dual-mode horn antenna as an array element in the 4×4 MAPAA was designed and produced to achieve side-lobe suppression and equal main beamwidth through an optimal selection of design parameters for the horn aperture.
3) Finally, we realized multi-beam pattern synthesis to simultaneously achieve low inner and outer SLLs by applying a GA-based evolutionary algorithm to the developed MAPAA.

This paper is organized as follows. In Section 2, we describe the pattern synthesis method of multi-beam array antennas in detail. In Section 3, the design method of the single horn antenna is presented. Simulated and measured results are shown in Section 4, and conclusions are drawn in Section 5.

2. FORMULATION OF MULTI-BEAM PATTERN SYNTHESIS

2.1. Multi-Beam Forming Formula for MAPAA

We consider an $M \times N$ planar array with a triangular lattice, as shown in Fig. 1. With reference to Fig. 1, D multiple signals are incident from each elevation and azimuth angle, $(\theta_d, \phi_d)_{d=1,\ldots,D}$ on the planar array. Although the MAPAA is a transmitting antenna system, the approach of a receiving system concept, as described in [11], is considered to formulate multiple beam patterns for convenience. Then, a column-ordered vector of the received signal $\mathbf{X}_d$ can be described as follows:

$$\mathbf{X}_d = \left[x_{11}^d x_{21}^d \ldots x_{M1}^d x_{12}^d \ldots x_{MN}^d \right]^T \tag{1}$$

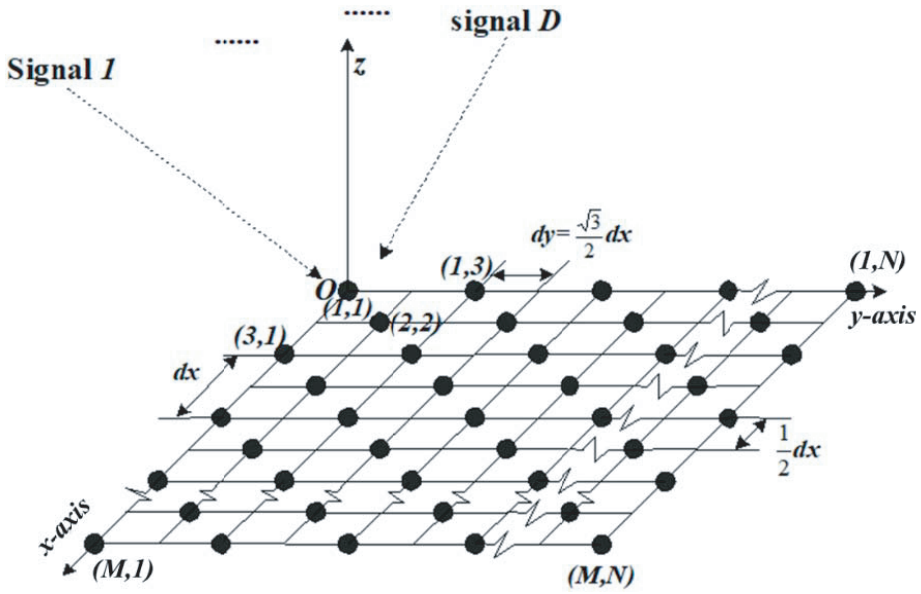

Figure 1. Planar array geometry with triangular lattice.

where x_{mn}^{d} means the received signal at each antenna element (m, n) and can be mathematically expressed as

$$x_{mn}^{d} = f_{mn} \sum_{d=1}^{D} [A_d \exp(jw_0 t) \cdot \exp[jk(d_{mn}^{y} \cdot v_d + d_{mn}^{x} \cdot u_d)]_{(m=1,\ldots,M,\ and\ n=1,\ldots,N)} \tag{2}$$

where k is a propagation constant; d_{mn}^{x} and d_{mn}^{y} are distances between the origin $\mathbf{O}$ and (m, n)th antenna elements in the x and y axes, respectively; $v_d = \sin\theta_d \sin\phi_d$, $u_d = \sin\theta_d \cos\phi_d$; A_d is each signal amplitude; T is the transpose operator; and w_0 is an operating frequency. We assume that, in this simulation, all the multiple signals have the same operating frequency. Finally, if the signal amplitudes have the same value A, the expected output signal vector $\mathbf{P}_d$ of the array antenna can be obtained as follows:

$$\mathbf{P}_d = \mathbf{C}^T \mathbf{X}_d = A \exp(jw_0 t) \cdot \mathbf{C}^T (\mathbf{F} \Theta \mathbf{S}_d) \tag{3}$$

where $\mathbf{C} = [c_{11}\ c_{21} \ldots c_{M1}\ c_{12} \ldots c_{MN}]^T$ is a weighting vector; $\mathbf{S}_d = [s_{11}^{d}\ s_{21}^{d} \ldots s_{M1}^{d}\ s_{12}^{d} \ldots s_{MN}^{d}]^T$ is the desired steering vector with $s_{mn}^{d} = \sum_{d=1}^{D} \exp[jk(d_{mn}^{y} \cdot v_d + d_{mn}^{x} \cdot u_d)]$; $\mathbf{F} = [f_{11}\ f_{21} \ldots f_{M1}\ f_{12} \ldots f_{MN}]^T$; and Θ denotes the dot product operator, respectively.

From Eq. (3), we define the generalized output signal $\mathbf{P}$ of an array antenna over the observation angle (θ, ϕ) as follows:

$$\mathbf{P} = \mathbf{C}^T \mathbf{X} = A \exp(jw_0 t) \cdot \mathbf{C}^T \mathbf{Y}, \tag{4}$$

where $\mathbf{Y} = [y_{11}\ y_{21} \ldots y_{M1}\ y_{12} \ldots y_{MN}]^T$ with $y_{mn} = f_{mn} \cdot \exp[jk(d_{mn}^{y} \cdot v + d_{mn}^{x} \cdot u)]$ ($v = \sin\theta \sin\phi$ and $u = \sin\theta \cos\phi$).

If we assume that $\mathbf{C} = \mathbf{W} \Theta \mathbf{S}_d^*$ and $\mathbf{P}' = |\mathbf{C}^T \mathbf{Y}|$, the radiation pattern of the array $\mathbf{P}'$ can be

described as follows:

$$\begin{aligned}\mathbf{P}'(u,v) &= \left|\mathbf{C}^T\mathbf{Y}\right| = \left|\left(\mathbf{W}\Theta\mathbf{S}_d^*\right)^T\mathbf{Y}\right| \\ &= \left|\begin{array}{l}\displaystyle\sum_{m=1}^{M}\sum_{n=1}^{N} f_{mn}w_{mn}\exp[jk(d_{mn}^y\cdot(v-v_1)+d_{mn}^x\cdot(u-u_1))] \\ \displaystyle+\sum_{m=1}^{M}\sum_{n=1}^{N} f_{mn}w_{mn}\exp[jk(d_{mn}^y\cdot(v-v_2)+d_{mn}^x\cdot(u-u_2))] \\ +\ldots \\ \displaystyle+\sum_{m=1}^{M}\sum_{n=1}^{N} f_{mn}w_{mn}\exp[jk(d_{mn}^y\cdot(v-v_D)+d_{mn}^x\cdot(u-u_D))]\end{array}\right| \\ &= \left|\sum_{m=1}^{M}\sum_{n=1}^{N} f_{mn}w_{mn}\left\{\sum_{d=1}^{D}\exp[jk(d_{mn}^y\cdot(v-v_d)+d_{mn}^x\cdot(u-u_d))]\right\}\right| \end{aligned} \tag{5}$$

where $\mathbf{W}$ is the complex weighting vector, $\mathbf{W} = [w_{11}\ w_{21}\ldots w_{M1}\ w_{12}\ldots w_{MN}]^T$, and the asterisk denotes the complex conjugate operator. As expected, the multi-beam pattern can be represented by linearly summing radiation patterns with each specific direction. If we further assume that each beam pattern can be independently controlled at the same time, and the antenna elements have an identical pattern one another, the multi-beam pattern of Eq. (5) can be modified as follows:

$$\mathbf{P}'(u,v) = \left|\begin{array}{l} f\displaystyle\sum_{m=1}^{M}\sum_{n=1}^{N} w_{mn}^1\exp[jk(d_{mn}^y\cdot(v-v_1)+d_{mn}^x\cdot(u-u_1))] \\ +f\displaystyle\sum_{m=1}^{M}\sum_{n=1}^{N} w_{mn}^2\exp[jk(d_{mn}^y\cdot(v-v_2)+d_{mn}^x\cdot(u-u_2))] \\ +\ldots \\ +f\displaystyle\sum_{m=1}^{M}\sum_{n=1}^{N} w_{mn}^D\exp[jk(d_{mn}^y\cdot(v-v_D)+d_{mn}^x\cdot(u-u_D))]\end{array}\right| \tag{6}$$

where W_{mn}^d $(d = 1,\ldots,D)$ represents the controllable complex weightings for each beam pattern. The design of the ABFM structure is based on Eq. (6) because four channels in the ABFM have their own digital phase shifter and attenuator, which can provide weightings for each beam direction to antenna elements through each channel, and the four channels are linearly combined to one output port of the ABFM via a Wilkinson power combiner and a solid state power amplifier.

2.2. Multi-Beam Optimization for MAPAA

In this subsection, to accomplish a low SLL for the MAPAA, an evolutionary optimization technique is applied to the previous formula of Eq. (6). The complex weightings w_{mn}^d can be expressed as follows:

$$w_{mn}^d = r_{mn}^d\exp(j\psi_{mn}^d)\ (d = 1,\ldots,D), \tag{7}$$

where r_{mn}^d and ψ_{mn}^d represent each amplitude and phase of antenna elements for the dth beam. Each phase of the antenna elements is optimized, while the amplitudes have fixed values during optimization procedure.

As stated earlier, a large SLL can be observed among multiple beam patterns when each beam is closely generated by one another within a limited scanning range. Therefore, simultaneous multi-beam optimization must be considered instead of independent optimization for each beam pattern. In order to synthesize a multi-beam pattern with a low SLL, the concept of subpopulation is adopted for each main beam [19]. In other words, subpopulations for each main beam separately evolve under the GA operators, such as crossover, mutation, and elitism. However, decoded values from the subpopulations are combined

to evaluate the fitness in one objective function. During optimization, a two-point crossover method including three chromosomes is used to achieve a fast convergence [20, 21]. Values for ψ_{mn}^{d} $(d = 1, \ldots, D)$ in the GA can be represented by a binary string or a real-valued string. In this paper, we select a binary string, and the gene is coded in 5 bits because the developed MAPAA has a 5-bit digital phase shifter. The cost function, J, to evaluate the fitness value of given individual in the $\phi = 0^{\circ}$ plane is defined as follows:

$$J = \min\left[\frac{1}{L}(g_a \cdot J_M + g_b \cdot J_S)\right], \tag{8}$$

where g_a and g_b are iteration gains,

$$J_M = \frac{1}{L_a}\sum_{l=1}^{L_a}\left|\frac{dp(u_l)}{p_r(u_l)}\right|^2 \ (l = 1, \ldots L_a), \tag{9}$$

$$with\ dp(u_l) = \left\{\begin{array}{ll} p_r(u_l) - p'(u_l), & u_l\ in\ each\ QdB\ main\ beamwidth \\ 0, & otherwise \end{array}\right\}\ in\ each\ mainlobe\ regions,$$

$$J_S = \frac{1}{L_b}\sum_{l=1}^{L_b}\left|\frac{dp(u_l)}{p_r(u_l)}\right|^2 \ (l = 1, \ldots L_b), \tag{10}$$

$$with\ dp(u_l) = \min[(p_r(u_l) - p'(u_l)), 0],\ u_l\ in\ the\ inner\ and\ outer\ sidelobe\ regions,$$

where $p_r(u_l)$ is the desired reference pattern, $p'(u_l)$ the multi-beam pattern in $u_l = \sin\theta_l$, and $L = L_a + L_b$, respectively. L_a means the normalization factor, which is the number of points for the radiation pattern plot in the given mainlobe regions, and L_b represents the normalization factors for the inner and outer sidelobe regions. For many simulation results, we found that the following equations between g_a and g_b can provide a suitable performance for our algorithm.

$$g_a + g_b < 5 \quad and \quad 1 < \frac{g_b}{g_a} < 2 \tag{11}$$

Here, we select the reference pattern $P_r(u)$, as shown in Fig. 2, in which the outer side-lobe and inner side-lobe regions are set to the desired low SLL, and the main-lobe shape can be specified to any type of parabola.

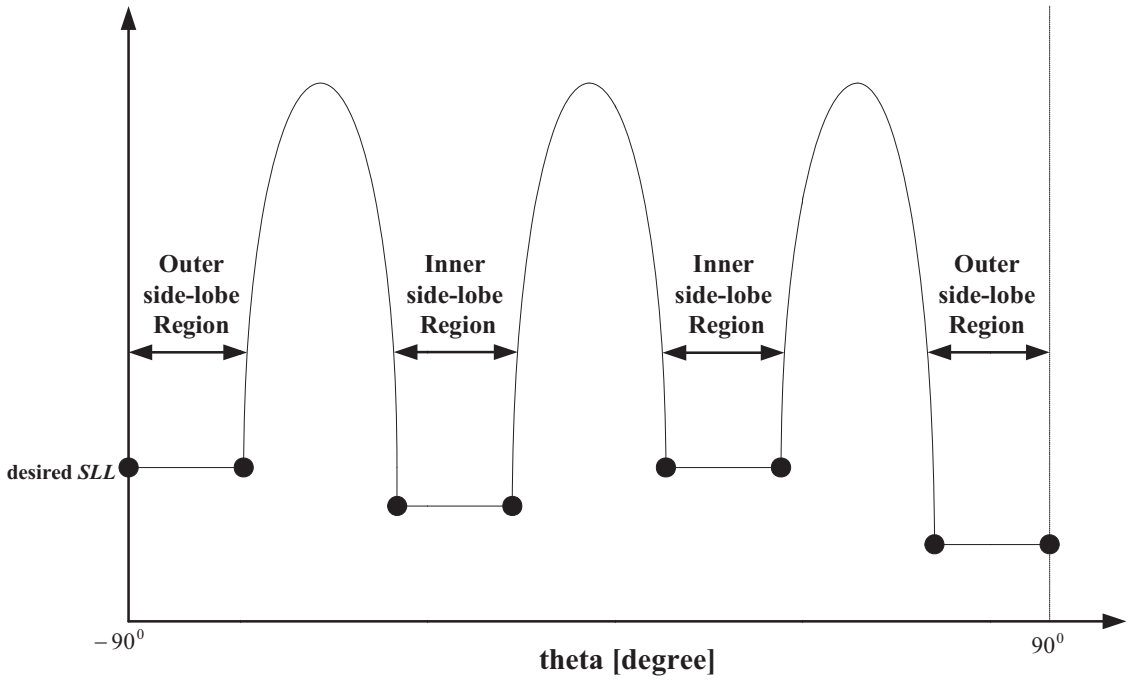

Figure 2. Reference pattern for the optimization of a multi-beam pattern.

The procedure for the multi-beam pattern synthesis using the GA is summarized as follows:

Step 1: Randomly generate initial subpopulations for each ψ_{mn}^{d} $(d = 1, \ldots, D)$, which represents each chromosome consisting of binary string.

Step 2: Calculate the fitness value using Eq. (8).

Step 3: Rank each chromosome from the best to the worst, according to their fitness values obtained by Step 2, and discard the bottom 50 percent.

Step 4: Create each new offspring setting from the selected top 50% using the two-point cross over operator.

Step 5: The best individual for each subpopulation from the present generation is saved, but it will not take part in the next step of the mutation process.

Step 6: Mutate the new offspring for each subpopulation based on the probability of mutation.

Step 7: Iterate from Steps 1 to 6 until the fitness value J is less than a predefined threshold value.

3. DUAL MODE HORN ANTENNA DESIGN

The desirable characteristics of beam axial symmetry, a low SLL, and low cross polarization can be obtained by designing a conical horn structure that supports TE_{11} and TM_{11} simultaneously [22]. The design parameters for the generation of dual modes are shown in Fig. 3. In order to control the relative amplitudes and phases of the two modes, the design parameters, such as the radii of the input a and output b, as well as the lengths, s and t, must be considered for an optimal design of the dual-mode horn. The radius a of the input waveguide must be selected to allow only the TE_{11} mode to propagate and the radius b of the output waveguide to allow both TE_{11} and TM_{11} modes to propagate. The TM_{11} mode generated by the internal bifurcation junction has little effect on the H-plane pattern but alters the field distribution of the dominant TE_{11} mode in the E-plane to be almost the same as that in the H-plane, which makes it possible to minimize diffractions at the aperture edges of the horn, especially those in the E-plane, by reducing the fields incident on the aperture edges. Therefore, the optimal selection of the dimensions for a side-lobe suppression and an equal beamwidth in the E- and H-planes can be realized by considering the field distributions on the horn aperture [23].

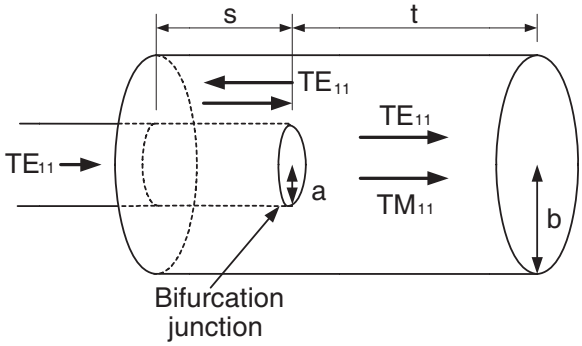

Figure 3. Design parameter for dual-mode generation of conical horn antenna.

4. EXPERIMENTAL RESULTS

In this section, we describe simulation and measurement results for the proposed MAPAA system. The manufactured transmitting MAPAA system is shown in Fig. 4, where it mainly consists of radiators, ABFMs, passive power distribution modules (PDM), active power distribution modules (ADM), and a system control unit (SCU) to control multi-beam pattern formation.

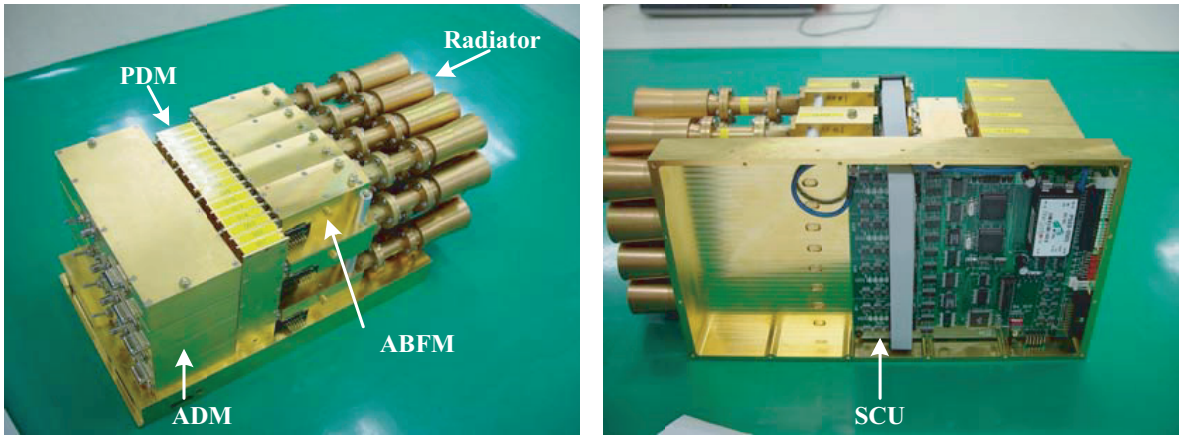

(a) (b)

Figure 4. Manufactured transmitting MAPAA system for multi-beam forming.

4.1. Dual Mode Horn Antenna

The circularly polarized dual-mode horn antenna consists of a conical horn with an aperture diameter of $1.9\lambda_0$ at 20.5 GHz and 8° half-flare angle, polarizer for left-handed circular polarization (LHCP), and transducer for mode conversion. The optimal dimensions for the horn antenna are given in Table 1. The radiation patterns measured using a far-field measurement facility at 20.5 GHz are also shown in Fig. 5. The equal main beamwidths in two planes orthogonal with each other are about ±50°.

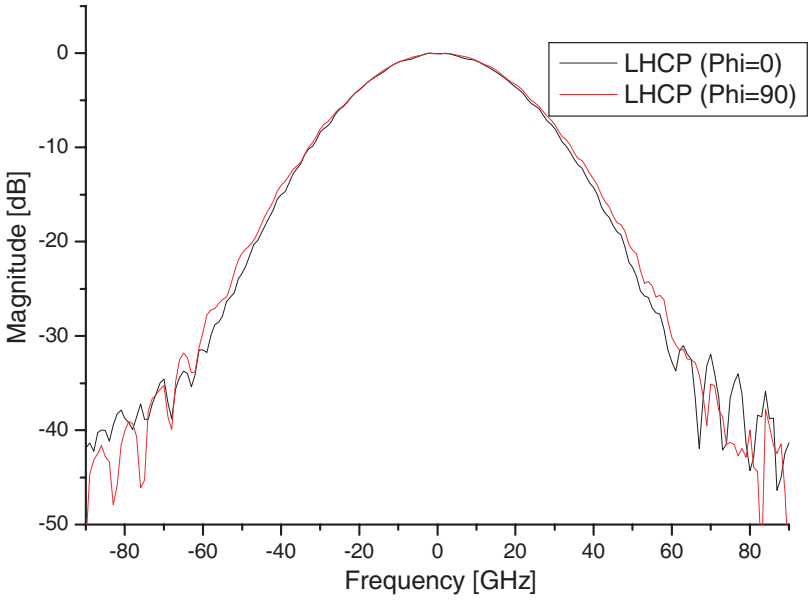

Figure 5. Radiation patterns measured and simulated at 20.5 GHz.

4.2. Optimization of Beam Patterns

In this subsection, we will show some simulated and measured results using the pattern synthesis method of Section 2 for both the single beam and multi-beam pattern.

Table 1. Optimal dimensions for the horn antenna.

Design Parameters	Optimum Value
s	4.45 mm
t	19.58 mm
a	7.61 mm
b	14 mm
Half-flare angle	8°

4.2.1. Generation of Multiple Beams

In order to measure multiple beam patterns for the transmitting antenna system, phases of each channel in the ABFMs must be initially adjusted using each phase shifter to be in-phase on the radiating apertures of the 4×4 array antenna. Fig. 6 shows the measured multiple beam patterns at the center frequency of 20.5 GHz when each main beam direction is given as follows:

- Beam 1: $(\theta_0, \phi_0) = (-10°, 0°)$
- Beam 2: $(\theta_0, \phi_0) = (-2°, 0°)$
- Beam 3: $(\theta_0, \phi_0) = (5°, 0°)$
- Beam 4: $(\theta_0, \phi_0) = (10°, 0°)$

In this figure, beam patterns overlap one another. As a result, the designed transmitting MAPAA can successfully provide independent multiple beam patterns.

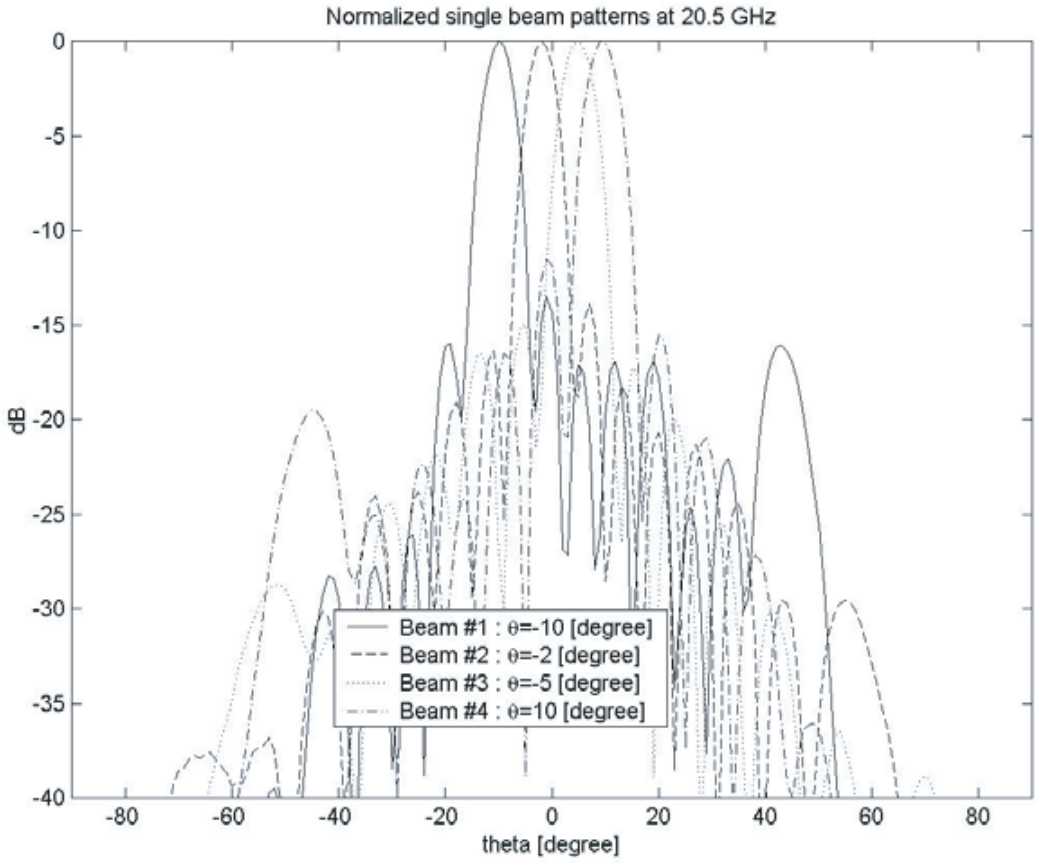

Figure 6. Measured result for the multi-beam forming of the MPAA.

4.2.2. Optimization of Single-Beam Pattern

We will show the simulation and measurement results of beam 4 among the four beams for the optimization of a single beam pattern. For single beam optimization, the cost function J of Eq. (8) is modified for simplicity as follows:

$$J = \max_{SLL} \left\{ 20 \log(\left|p'(u_l)\right|) \right\}, \quad u_l \textit{ in the sidelobe region.} \tag{12}$$

In order to reduce a maximum SLL (MSLL) of a single beam pattern using Eq. (12), GA parameters were determined as follows: population size for the single beam was set to three times the length of each chromosome, a probability of crossover to 0.8 and that of mutation to 0.025. Fig. 7 shows the simulation results for beam 4 of the MAPAA. Case 1 represents the optimized radiation pattern at a center frequency of 20.5 GHz for beam 4 using the synthesis method in Section 2, and Case 2 denotes the initial radiation pattern of beam 4. When the main beam direction of the beam 4 is scanned to $\theta_0 = 5^\circ$ in the $\phi = 0^0$ plane, the related radiation patterns including the optimized result are plotted in Fig. 8.

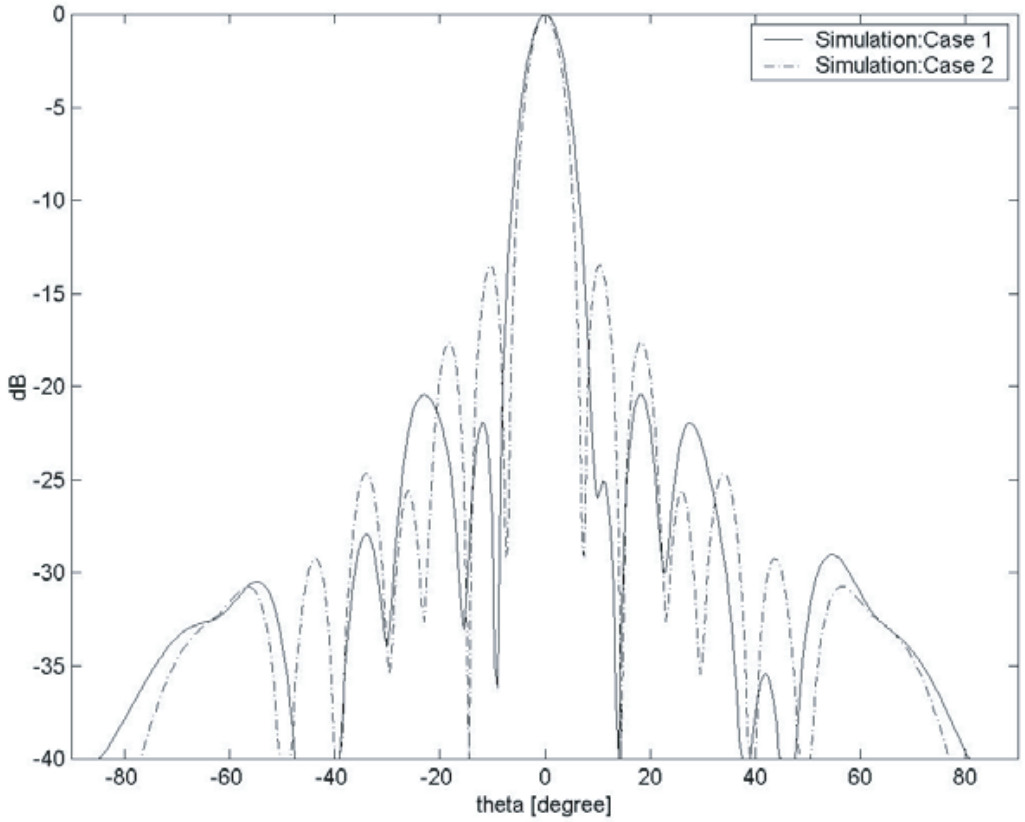

Figure 7. Simulation result of the optimized single beam pattern at the boresight.

The MSLLs and 3 dB main-lobe beamwidths (MLBs) for beam 4 are compared and summarized in Table 2. In comparison of the simulation and measurement results, the optimized beam patterns can provide lower SLL than the initial ones, as shown in Table 2.

4.2.3. Optimization of Multi-beam Pattern

In this section, beam 2 and beam 4 among the four beams of the MAPAA are simultaneously considered to generate a multi-beam pattern at the same frequency. Case 2 of Fig. 9 shows the initial multi-beam pattern at the center frequency of 20.5 GHz. For this example, the main beam direction of beam 2 is given as $(\theta_0, \phi_0) = (-10^\circ, 0^\circ)$, and that of beam 4 is set to $(10^\circ, 0^\circ)$. When two beams are closely

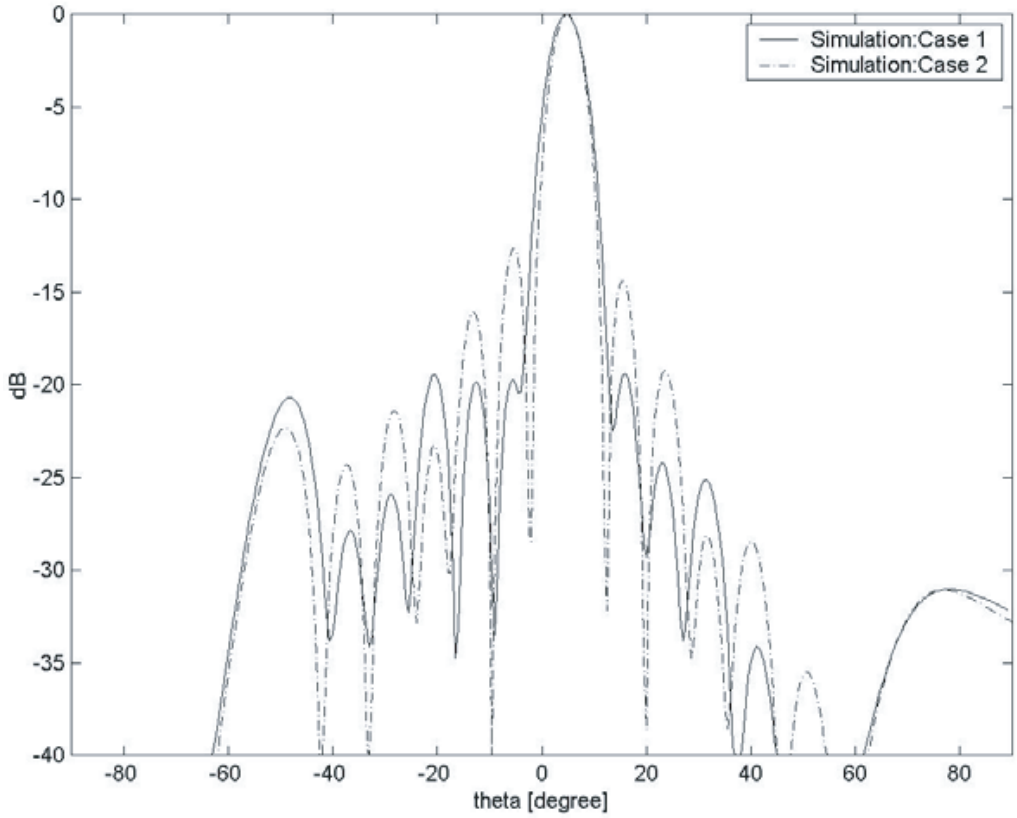

Figure 8. Simulation result of the optimized single beam pattern when the main beam is θ_0 scanned to $\theta_0 = 5°$ in the plane.

Table 2. Comparison of maximum side-lobe levels for the single beam patterns. Case 1: Optimized radiation pattern for the beam 4. Case 2: Initial radiation pattern for the beam 4.

Items for single beam pattern			Simulation		Measurement	
			Case 1	Case 2	Case 1	Case 2
Maximum radiation angle, θ_0 at $\phi = 0°$	0°	3 dB *MLB*	7.2°	6.34°	7.52°	6.34°
		MSLL	−20.4 dB	−13.47 dB	−19.25 dB	−13.22 dB
	5°	3 dB *MLB*	7.14°	6.39°	7.14°	6.29°
		MSLL	−19.39 dB	−12.60 dB	−18.02 dB	−12.40 dB

generated at the same time, a large inner side-lobe is observed, as shown in this figure. In order to reduce both the inner and outer SLLs of the initial beam pattern, the proposed method is applied to the optimization of the initial multi-beam pattern. For the multi-beam pattern synthesis method, we set the iteration gains, g_a and g_b, to 1.2 and 1.5, subpopulation size for each beam to three times the length of each chromosome, each probability of crossovers to 0.82, and those of mutations to 0.02. In the desired reference pattern, the inner and outer SLLs are set to −20 dB and −25 dB, respectively. In addition, a 10 dB beamwidth in Eq. (12) is selected for this measurement. Case 1 of Fig. 9 shows the optimized multi-beam pattern for the initial pattern. The result of Case 1 was derived after 27 generations. In comparison with the initial multi-beam pattern, an approximately 10 dB reduction of the inner SLL was achieved with the optimized one. It can be expected that, although a 4×4 array antenna is used in this example, a further reduction of outer SLL as well as the inner SLL can be achieved, as the number of arrays is increased.

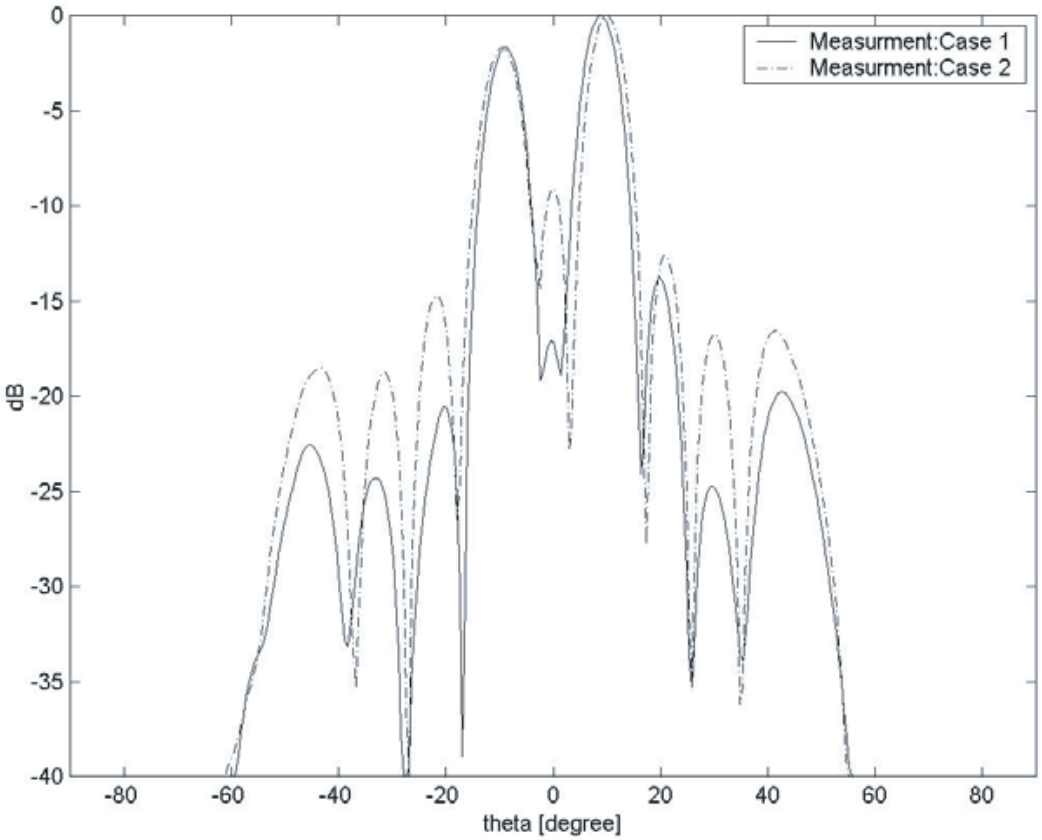

Figure 9. Measured result of the optimized multi-beam pattern.

5. CONCLUSION

This paper describes the results of beam forming and optimization for both the single beam and multi-beam of the Ka-band MAPAA. In addition, the dual-mode horn antenna with an aperture diameter of $1.9\lambda_0$ at 20.5 GHz and half-flare angle of 8° is designed. The simulated and measured results for the designed antenna are compared and show a good agreement with each other. In the case of beam forming, the 4×4 MAPAA was designed to provide four spot beams at the Ka-band, and from the measured result, we observed that the four beams were independently and successfully generated. In this study, when two beams are simultaneously generated at the same frequency, a large inner side-lobe can appear between two main beams. To improve the initial multi-beam pattern in terms of side-lobe reduction, the formulation for a multi-beam was derived, and the evolutionary optimization technique was applied to provide optimal phases of each channel in the ABFMs to the corresponding multiple beams. The results show that the optimized multi-beam pattern can achieve lower inner and outer SLLs simultaneously than the initial one.

In future work, we plan to extend this study by combining more sub-array modules based on the currently developed 4×4 MAPAA and forming more simultaneous multi-beams. We will continue to work on applying and analyzing other advanced optimization techniques, such as the particle swarm optimization method with high computational efficiency, to more complex MAPAA systems for multi-beam forming optimization.

ACKNOWLEDGMENT

This work was supported by research grants from the Daegu Catholic University in 2020.

REFERENCES

1. Regier, F. A., "The ACTS multibeam antenna," *IEEE Trans. on Microwave and Techniques*, Vol. 40, No. 6, 1159–1164, June 1992.
2. Verma, S. and E. Wiswell, "Next generation broadband satellite communication systems," *21th AIAA International Communications Satellite Systems Conference and Exhibit*, Yokohana, Japan, April 15–19, 2003.
3. Wang, Y., C. Wang, P. Lian, S. Xue, J. Liu, W. Gao, Y. Shi, Z. Wang, K. Yu, X. Peng, B. Du, and S. Xiao, "Effect of temperature on electromagnetic performance of active phased array antenna," *Electronics*, Vol. 9, 1–13, July 2020.
4. Paris, A., I. Del Portillo, B. Cameron, and E. Crawley, "A genetic algorithm for joint power and bandwidth allocation in multibeam satellite systems," *2019 IEEE Aerospace Conference*, 1–15, Big Sky, USA, March 2–9, 2019.
5. Wang, L., X. Hu, S. Ma, S. Xu, and W. Wang, "Dynamic beam hopping of multi-beam satellite based on genetic algorithm," *2020 IEEE Intl. Conf. on Parallel & Distributed Processing with Applications, Big Data & Cloud Computing, Sustainable Computing & Communications, Social Computing & Networking (ISPA/BDCloud/SocialCom/SustainCom)*, 1364–1370, Exeter, United Kingdom, December 17–19, 2020.
6. Kadambar, S., A. Goyal, and A. K. Reddy Chavva, "Millimeter wave multi-beam combining algorithm for efficient 5G cell search," *2020 IEEE 17th Annual Consumer Communications & Networking Conference (CCNC)*, 1–6, Las Vegas, USA, March 26, 2020,
7. Kim, S., G. Kwon, and H. Park, "High-resolution multi-beam tracking with low overhead for mmWave beamforming system," *ICT Express*, Vol. 7, No. 1, 28–35, 2021.
8. Satch, T., "Dielectric-loaded horn antenna," *IEEE Trans. on Antennas and Propagation*, Vol. 20, 199–201, March 1972.
9. Mac, B. and A. Thomas, "Design of corrugated conical horns," *IEEE Trans. on Antennas and Propagation*, Vol. 26, 369–372, March 1978.
10. "ANSYS HFSS: Everything to Know," Accessed: Jan. 4. 2020, [Online], Available: https://sunglass.io/ansys-hfss/.
11. Katoch, S., S. S. Chauhan, and V. Kumar, "A review on genetic algorithm: Past, present, and future," *Multimedia Tools and Applications*, Vol. 80, 8091–8126, October 2020.
12. Balanis, C. A., *Antenna Theory Analysis and Design*, 4th Edition, John Wiley & Sons, Inc., 2016.
13. Makarov, S. N., V. Lyer, S. Kulkarni, and S. R. Best, *Antenna and EM Modeling with MATLAB*, 2th Edition, John Wiley & Sons, Inc., 2021.
14. Bray, M. G., D. H. Werner, D. W. Boeringer, and D. W. Machuga, "Optimization of thinned aperiodic linear phased arrays using genetic algorithms to reduce grating lobes during scanning," *IEEE Trans. on Antennas and Propagation*, Vol. 50, No. 12, 1732–1742, December 2002.
15. Bae, J.-H., K.-T. Kim, and C.-S. Pyo, "Design of steerable linear and planar array geometry with non-uniform spacing for side-lobe reduction," *IEICE Trans. on Communications*, Vol. E88-B, No. 1, 345–357, January 2005.
16. Hua, D., W. Li, and X. Shi, "Pattern synthesis for large planar arrays using a modified alternating projection method in an affine coordinate system," *Progress In Electromagnetics Research M*, Vol. 39, 53–63, 2014.
17. Mateo, R.-V., A. S.-S. Aaron, A. R.-G. Juan, E. L.-M. Maria, and J. A.-P. Francisco, "Optimizing radiation patterns of thinned arrays with deep nulls fixed through their representation in the Schelkunoff unit circle and a simulated annealing algorithm," *Sensors*, Vol. 22, No. 3, 1–15, February 2022.
18. Lee, J.-M., J.-H. Bae, N.-S. Seong, and C.-S. Pyo, "Active phase shifter module for satellite communications at Ka-band," *IEEE Antennas and Propagation Society Symposium*, 1–4, Monterey, CA, USA, June 20–25, 2004.
19. Yahya, R.-S. and E. Michielssen, *Electromagnetic Optimization by Genetic Algorithm*, John Wiley & Sons, Inc., 1999.

20. Choo, H. and H. Ling, "Design of multiband microstrip antennas using a genetic algorithm," *IEEE Microwave and Wireless Components Letters*, Vol. 12, No. 9, 345–347, September 2002.
21. Mehboob, U., J. Qadir, S. Ali, and A. Vasilakos, "Genetic algorithms in wireless networking: Techniques, applications, and issues," *Soft Computing*, Vol. 20, 2467–2501, February 2016.
22. Potter, P. D., "A new horn antenna with suppressed sidelobes and equal beamwidth," *Microwave J.*, Vol. 6, 71, 1963.
23. Collin, R. E., *Antennas and Radiowave Propagation*, McGraw-Hill, 1985.